Wideband Spatial Channel Model in an Urban Cellular Environments At 28 GHz

Sooyoung Hur[1], Yeon-Jea Cho[2],
Taehwan Kim[2], JeongHo Park[1],
[1] Samsung Electronics, Korea
{sooyoung.hur, jeongho.jh.park}@samsung.com
[2] KAIST, Korea

Andreas F. Molisch[3], Katsuyuki Haneda[4],
and Michael Peter[5],
[3] University of Southern California, USA
[4] Aalto University, Finland
[5] Fraunhofer Heinrich Hertz Institute, Germany

***Abstract*—This paper presents channel propagation measurements and analysis of the channel characteristics of millimeter wave (mmWave) transmission for urban cellular communication systems, in particular in the promising 28 GHz band. For channel propagation analysis, the urban measurement campaign was conducted with a synchronously spherical scanning 28 GHz channel sounder system, from which omni-like channel measurements are obtained for channel modeling. From the measurements, we analyze the spatio-temporal channel characteristics such as multipath delay, angular statistics, and pathloss. The clustering analysis has been done including its power distribution. Then, a set of millimeter wave radio propagation parameters is presented, and the corresponding channel models based on the 3GPP spatial channel model (SCM) are also described.**

***Index Terms*—mmWave, 28GHz, channel measurement, propagation, SCM, channel model.**

I. Introduction

The millimeter wave band will be a key enabling component for fifth generation cellular communication systems (5G) to obtain more spectrum [1], [2] and to support more data traffic for various multimedia service. The understanding of channel propagation characteristics in the new spectrum is essential for developing 5G technology.

Many channel measurement campaigns and studies of the channel characteristics in millimeter wave band have been done. Millimeter wave systems require a large directional gain in order to combat their relatively high pathloss compared to systems at lower frequencies. To assess the feasibility of millimeter wave for outdoor cellular access communications, some measurement campaigns were conducted using the directional channel sounder in Manhattan, New York and Austin, Texas [3], [4]. Also, research projects including industry and academy, such as METIS [5] and MiWEBA [6], have been launched to develop a proper 5G channel propagation model including the mmWave spectrum. However, currently there is no channel model at mmWave including both delay and direction at both link ends,, i.e., double-directional wideband channel model. In this paper, we focus on characterizing the channel in the 28 GHz mmWave band.

The proposed channel sounder system in [7] can measure the omni-like channel information by synthesizing angular power delay profiles (PDPs). Because the channel sounder operates synchronously between transmitter and receiver and records the time-stamps, each angular PDP can be aligned in time using the propagation time information per measurement. Using this approach, the characteristics of millimeter wave band can be analyzed based on the synthesized omni-directional PDPs. To extract the channel parameters from measurements, we adapt the methodology of the statistical spatial channel model used in WINNER II [8] and 3GPP SCM [9].

This paper presents the most up-to-date developments and measured results for achieving a complete 28 GHz omni-directional spatial channel model for Non-Line-of-Sight (NLoS) locations, based on wideband propagation measurements collected in an urban area, Daejeon, Korea. We investigate how waves in the 28 GHz band propagates in outdoor urban environment based on the extensive measurement campaign. As a result, we propose the initial channel model on 28GHz mmWave band in urban cellular scenarios, which can model statistics for double-directional channel models.

II. Measurement Campaign in Urban Scenario

The measurement campaign is performed in an urban environment in Daejeon, Korea. In the campaign, both line-of-sight (LoS) and non line-of-sight (NLoS) locations are selected in various positions on the street. Fig. 1 shows a bird's eye view of the urban area, with transmitter and receiver locations marked; distance between transmitter and receiver was up to 200 m. The synchronous channel sounder system described in [7] was used for channel measurements. Note that the sounder system is resolvable up to 4 nano second separations between paths with 250 MHz bandwidth, and equipped with high gain horn (24.5 dBi) antennas with 10° 3dB beamwidth. The signal is transmitted with up to 29 dBm. The transmitter was placed on the fifth floor (15m above the ground) of the seventh-story building and the azimuth and elevation angle range of the transmitter horn antenna was set in the range of $-60°$ to $60°$ and $-40°$ to $10°$, respectively. On the other hand, the azimuth and elevation angle range of the receiver horn antenna was from $0°$ to $360°$ and $-60°$ to $60°$, respectively. After post-processing the angular PDPs, the omni-directional measurements were synthesized for mmWave channel modeling. The details of the post-processing are presented in [7]. In the measurement campaign, channels were recorded at more

Fig. 1. Map of the measurement campaign in urban area

than 30 different Rx locations, however, only 11 Rx locations turned out to be valid to obtain omni-directional PDPs due to the signal outage in other Rx locations.

III. mmWave Channel Modeling

We focus on NLoS environments for the channel modeling first because the NLoS condition is more critical in mmWave cellular communications.

1) Propagation Loss Analysis: From the received power of omni-measurements, the relative pathloss with the received power at the reference distance ($8m$ reference distance on the measurement campaign) is calculated, then the absolute pathloss model is derived by adjusting the referenced pathloss model from the Friis's transmission model. The measured values of the pathloss (averaged over small-scale fading) are shown in Fig. 2. The pathloss model is formally expressed as:

$$\begin{aligned} PL\left(d\right)\left[dB\right] &= \overline{PL}\left(d\right) + X_\sigma \\ &= \overline{PL}_F\left(d_0\right) + 10\,n\,\log\left(\frac{d}{d_0}\right) + X_\sigma \end{aligned} \tag{1}$$

where $\overline{PL}_F\left(d_0\right)$ represents the free space path loss (FSPL) at the reference distance d_0 and the linear slope n is the path loss exponent. The FSPL $\overline{PL}_F\left(d_0 = 8\right)$ $(= 79.46$ dB$)$ is computed by the well-known Friis's transmission equation. Following the approach of [10], we choose a reference distance of d_0 for the line-fitting. It gives a path loss exponent 3.53 in the NLoS conditions and it is scattered with a random shadowing effect. Here, X_σ, which reflects a random shadowing effect, is a Gaussian random variable (in dB) with mean 0 and variance σ^2.

Due to the limitation of the measurement system, the measurable pathloss is around 140 dB in the urban measurement campaign, and only 11 different channels are valid to synthesize omni-directional PDPs and to calculate the pathloss values. The other locations which received signal was not detectable are considered as outage area with more than 140 dB pathloss. The analysis of path loss and SCM parameters is performed only on the valid Rx locations. Such a path loss model conditioned on the valid Rx locations should

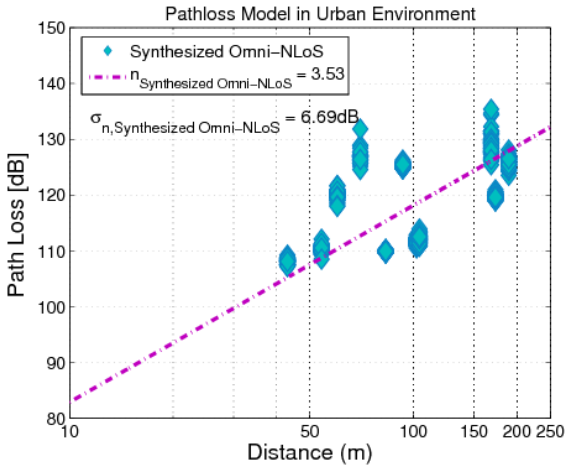

Fig. 2. Pathloss model and scatter plots for Urban Scenario measured in Daejeon, Korea

be well combined with the corresponding outage probability model later. Currently, all measured channels on the outage measurement are excluded for modeling procedures in this paper. Further, the reliability of the current path loss model could be improved by applying the statistical path loss model [11], [12] especially in 28 GHz cellular systems due to the fact that the channel characteristic of 28 GHz is more sensitive to surrounding environments than the current cellular frequencies operating at below 6GHz.

2) Spatio-Temporal Analysis: The parameters of delay and angular information are extracted from the measurements, and the mmWave channel is parameterized with a statistical model, such as log-normal distribution of delay spread. Adapting the SCM framework, the cluster-based channel parameters in the spatio-temporal domain are analyzed after finding clusters with the K-Power-Means algorithm. The inter/intra-cluster parameters are evaluated as defined in [9].

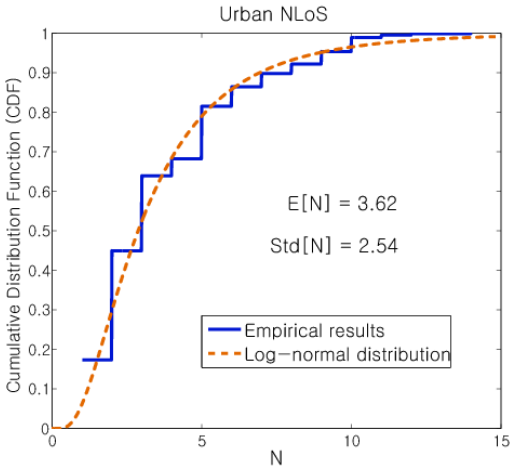

Fig. 3. Cumulative distribution function of the number N of clusters for Urban Scenario measured in Daejeon, Korea

The number of clusters, N, depends on propagation scenarios.Given the measured urban scenario, the average number of

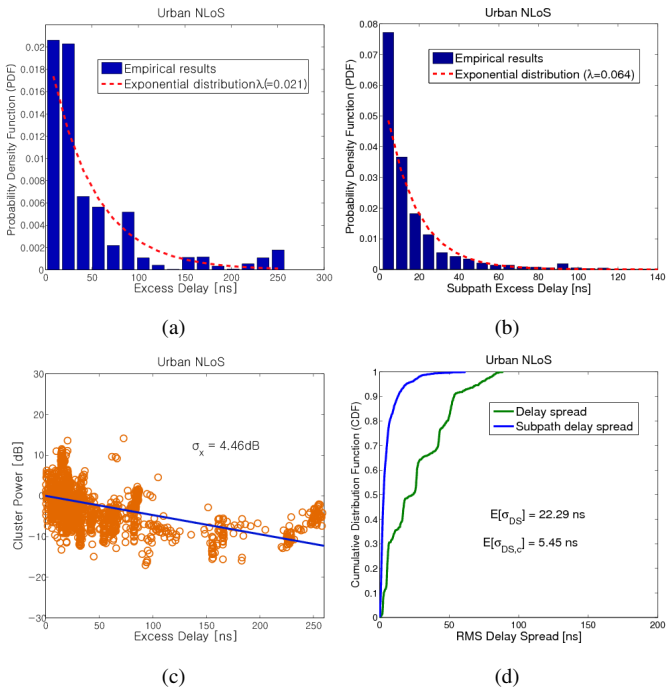

Fig. 4. (a) Probability density function of excess delays for Urban NLoS environment, (b) probability density function of subpath delays for Urban NLoS environment (c) power delay spectrum, (d) cumulative distribution functions of RMS delay and subpath delay spreads.

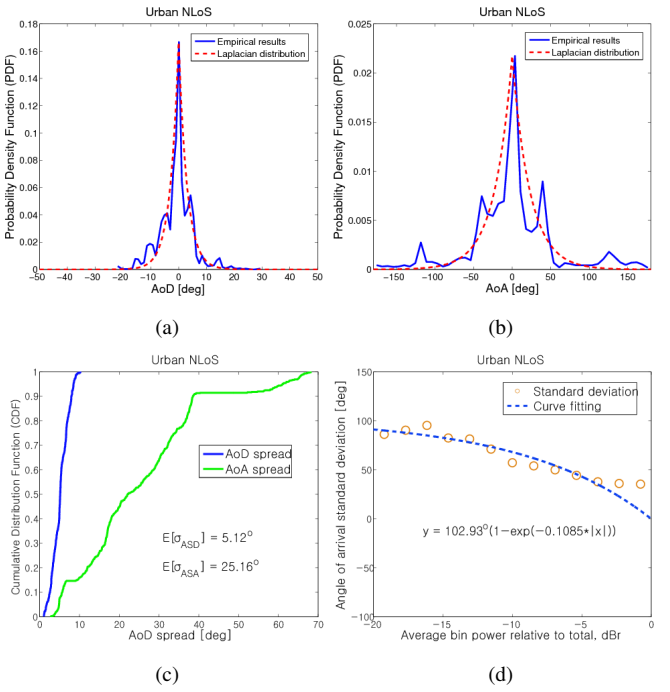

Fig. 5. (a) Probability density function of the cluster AoD, (b) probability density function of the cluster AoA (c) cumulative distribution functions of AoD and AoA spreads, (d) AoA standard deviation versus average bin power relative to total received power.

clusters at 28 GHz is 3.62 with standard deviations of 2.54. The corresponding cumulative distribution functions (CDFs) of the number of clusters are shown in Fig. 3. The statistics of the measured N is fitted to the log-normal distribution.

The temporal channel characteristics are analyzed with the synthesized omni-directional PDPs, and the excess delay of clusters, RMS delay spread, and the power-delay spectrum are characterized by their statistical distributions. Fig. 4(a) and Fig. 4(b) show that both cluster and subpath delays (in other words, inter-cluster and intra-cluster delays) are all exponentially distributed in the measured urban scenario. Also, Fig. 4(c) shows the single-slope exponential decay of the cluster powers. The RMS delay and subpath delay spreads, σ_{DS} and $\sigma_{DS,c}$, follow the WINNER II definition [13] and their CDF properties are illustrated in Fig. 4(d). The majority of measured channels have an RMS delay spread below 100 ns in the urban scenario of interest.

In this paper, limited elevation-angle resolution, the spatial channel characteristics are analyzed only in azimuth. Note that the angle resolution in observed channels is limited to 10 degree in azimuth angle due to the limitation on channel sounder [7] First, the statistics of angles are analyzed. Fig. 5(a) and Fig. 5(b) show PDFs of the measured cluster angle-of-departure (AoD) and the cluster angle-of-arrival (AoA) in the urban environment, where Laplacian distributions are overlaid as the best fit for the measurement data. The AoD and the AoA spreads (σ_{ASD} and σ_{ASA}) are illustrated in Fig. 5(c) along with their CDFs. The average AoD and AoA spreads in the urban scenario are 5.12° and 25.16°, respectively.

From the measured data, there is a relationship between direction and path-power, namely that the standard deviation of each cluster direction depends on the relative cluster power in the measurement . Fig. 5(d) illustrates the curve fit for the standard deviations of the AoA obtained using uniformly spaced bins of the received power in the urban environment. The corresponding standard deviation, $\sigma_{n,AoA}$, can be expressed as follows:

$$\sigma_{n,AoA} = A \cdot (1 - \exp(B \cdot |P_{n,dBr}|)), \quad (2)$$

where $P_{n,dBr} < 0$ is the relative power of the nth cluster in dBr with respect to the total received power and the parameters A and B are dependent on a specific scenario.

From the spatio-temporal analysis, statistical characteristics of mmWave channel is parameterized and modeled. Due to the page limitations, only a part of the entire results are covered in this paper, and more detailed analysis will be introduced in [14].

IV. mmWave Channel Modeling and Verification

A. Channel Modeling

In this subsection, we summarize the steps for generating all MPCs to simulate small scale fading in NLoS environments. Procedures similar to 3GPP SCM [9] and WINNER II model [13] are applied on the basis of measurement results and the model is extended to cover mmWave systems up to 250 MHz bandwidth with our proposed subpath delay/AoD/AoA distributions. Note that the model is valid in UMi scenario,

which is modeled up to 200m in the separation between Tx and Rx.

1) Large scale parameters:

For notational convenience we define six cross-correlation coefficients between the four large scale parameters as follows: $\rho_{12} \triangleq \rho(\log\sigma_{DS}, X_\sigma) = 0.2891$, $\rho_{13} \triangleq \rho(\log\sigma_{ASD}, X_\sigma) = 0.0070$, $\rho_{14} \triangleq \rho(\log\sigma_{ASA}, X_\sigma) = 0.2389$, $\rho_{23} \triangleq \rho(\log\sigma_{ASD}, \log\sigma_{DS}) = 0.6549$, $\rho_{24} \triangleq \rho(\log\sigma_{ASA}, \log\sigma_{DS}) = 0.8273$, and $\rho_{34} \triangleq \rho(\log\sigma_{ASD}, \log\sigma_{ASA}) = 0.5678$. The large scale parameters are multiplied with a transform matrix to impose cross correlation between them:

$$\mathbf{T} = \begin{bmatrix} 1 & \rho_{12} & \rho_{13} & \rho_{14} \\ \rho_{12} & 1 & \rho_{23} & \rho_{24} \\ \rho_{13} & \rho_{23} & 1 & \rho_{34} \\ \rho_{14} & \rho_{24} & \rho_{34} & 1 \end{bmatrix}^{1/2}, \tag{3}$$

where the square root matrix is generated using the Cholesky decomposition. Using the transform matrix $\mathbf{T}$, correlated Gaussian random variables are generated following the WINNER model procedures [13]. Then, the RMS DS, AoD spread, AoA spread and shadow fading are realized as log-normal random variables with parameters summarized in Table. I

2) Cluster delays: With the correlated delay spread generated in the previous step, random delays $(\tilde{\tau}_1, \ldots, \tilde{\tau}_N)$ for each cluster are determined by

$$\bar{\tau}_n = -r_{DS}\sigma_{DS}\ln y_n, \quad n = 1, \ldots, N, \tag{4}$$

where y_n $(n = 1, \ldots, N)$ are i.i.d. random variables with uniform distribution $\mathcal{U}(0, 1)$. The generated delays are ordered in a descending manner so that $\tilde{\tau}_N > \tilde{\tau}_{N-1} > \cdots > \tilde{\tau}_1$. The delays are normalized as

$$\tau_n = \tilde{\tau}_n - \tilde{\tau}_1, \tag{5}$$

for $n = 1, \ldots, N$.

3) Cluster powers: Each cluster power, which is defined as sum of all path powers in a cluster, is obtained by

$$P_n'(\tau_n) = \exp\left(-\tau_n\left(\frac{r_{DS}-1}{r_{DS}\sigma_{DS}}\right)\right)\cdot 10^{-X_n/10}, \tag{6}$$

where X_n $(n = 1, \ldots, N)$ are i.i.d. Gaussian random variables with mean 0 and standard deviation σ_X, which reflects a random shadowing effect on the per-path powers. (Refer to Fig. 4(d) for the value σ_X) Then, path powers are normalized so that the total path power for all N paths is equal to

$$P_n(\tau_n) = \frac{P_n'(\tau_n)}{\sum_{n=1}^{N} P_n'(\tau_n)}. \tag{7}$$

4) Cluster AoAs: From the cluster angular characteristics shown in Fig. 5, it is useful to model the cluster AoA as a function of its relative power, which can be mathematically formulated by the inverse Laplacian function. In this regard, random mean AoAs $(\varphi_{1,AoD}, \ldots, \varphi_{N,AoD})$ for each of the N clusters can be determined by

$$\varphi_{n,AoA} = U_n\tilde{\varphi}_{n,AoA} + V_n, \quad n = 1, \ldots, N, \tag{8}$$

where

$$\tilde{\varphi}_{n,AoA} = -K_{ASA}\sigma_{ASA}\ln\left(\frac{P_n}{\max(P_n)}\right). \tag{9}$$

Here, U_n is a discrete random variable with the set of $\{-1, 1\}$ and V_n is the Gaussian random variable with mean 0 and standard deviation $\sigma_{ASA}/7$.

5) Cluster AoDs: Similarly to the cluster AoA as described above, random mean AoDs $(\varphi_{1,AoA}, \ldots, \varphi_{N,AoA})$ for each of the N clusters can be generated according to

$$\varphi_{n,AoD} = U_n\tilde{\varphi}_{n,AoD} + V_n, \quad n = 1, \ldots, N, \tag{10}$$

where

$$\tilde{\varphi}_{n,AoD} = -K_{ASD}\sigma_{ASD}\ln\left(\frac{P_n}{\max(P_n)}\right). \tag{11}$$

6) Subpath delays (mmWave band extension): For the deterministic subpath delay model originally proposed in [9], [13], the mth subpath delays of the nth cluster is generated from the following formula:

$$\tau_{n,m} = \tau_n + \sigma_{DS,c}\cdot\alpha_m, \tag{12}$$

where $m = 1, \ldots, M$ and α_m is obtained from Table II.

7) Subpath AoDs and AoAs: For the deterministic subpath AoD and AoA models, the mth subpath AoD and AoA of the nth cluster are respectively generated from the following formulas

$$\varphi_{n,m,AoD} = \varphi_{n,AoD} + \sigma_{AoD,c}\cdot\beta_m, \tag{13}$$

$$\varphi_{n,m,AoA} = \varphi_{n,AoA} + \sigma_{AoA,c}\cdot\beta_m, \tag{14}$$

where $m = 1, \ldots, M$ and β_m is obtained from Table II.

The key SCM parameters mentioned in this section are shown in Table I for the urban NLoS measurement scenario.

TABLE II
SUBPATH DELAY AND ANGLE OFFSETS WITHIN A CLUSTER FOR 1 RMS DELAY AND ANGLE SPREADS (M = 10)

Subpath number, m	Offset delays α_m [ns]	Offset angles β_m [°]
	Exponential distribution	Laplace distribution
1, 2	0 / 0.0502	± 0.0318
3, 4	0.1393 / 0.2485	± 0.2034
5, 6	0.3857 / 0.5621	± 0.4463
7, 8	0.7985 / 1.1394	± 0.8951
9, 10	1.7148 / 3.4265	± 1.9894

TABLE I
KEY SCM PARAMETERS FOR THE URBAN NLOS MEASUREMENT SCENARIO (N = 4, M = 10)

	μ_{DS}	ε_{DS}	r_{DS}	μ_{ASD}	ε_{ASD}	μ_{ASA}	ε_{ASA}	K_{ASD}	K_{ASA}	$\sigma_{ASD,c}$	$\sigma_{ASA,c}$	$\sigma_{DS,c}$	ρ_{12}	ρ_{13}	ρ_{14}	ρ_{23}	ρ_{24}	ρ_{34}
Urban	-7.893	0.488	1.309	0.675	0.203	1.304	0.314	1.582	1.828	4.23°	8.84°	5.45 ns	0.2891	0.0070	0.2389	0.6549	0.8723	0.5678

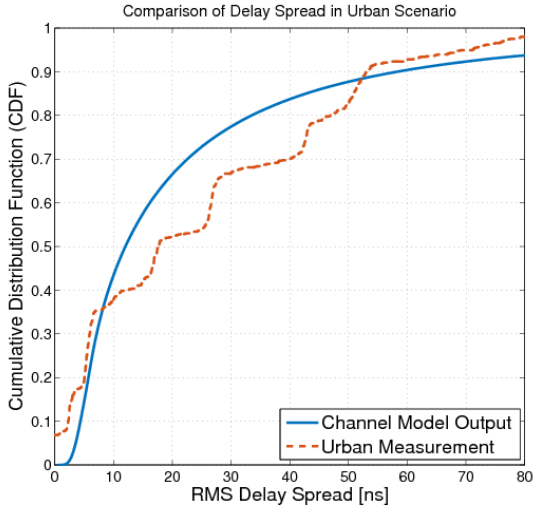

(a)

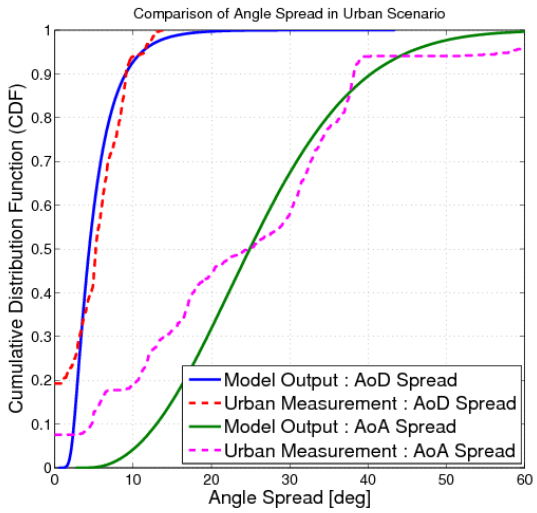

(b)

Fig. 6. Comparison of the measurement data and the proposed model: (a) Delay Spread, (b) Angle Spread Departure and Arrival

B. Channel Model Verification

The channel model based on the measurement campaign is verified by comparison with the original measurement data. We checked the delay spread and AoA/AoD spreads of the channel model output and the measurements. Fig. 6 shows the comparison of the CDFs of these parameters, and find it is reasonably matched for the delay spread. However, the angle spread is mismatched in low values, because of the deficient number of measurable paths on measurement data.

V. CONCLUSION

In this paper, we analyzed the radio propagation characteristics at 28 GHz based on a measurement campaign with a synchronous channel sounder system. Essential channel parameters were successfully extracted and modeled using the measurement data and furthermore the corresponding channel model for the urban scenario is also presented. The presented 28 GHz model will be continuously updated by performing additional measurement campaigns and by refining the accuracy of parameter statistics through better modeling methodologies.

REFERENCES

[1] W. Roh, J.-Y. Seol, J. Park, B. Lee, J. Lee, Y. Kim, J. Cho, K. Cheun, and F. Aryanfar, "Millimeter-Wave Beamforming as an Enabling Technology for 5G Cellular Communications: Theoretical Feasibility and Prototype Results," *IEEE Communications Magazine*, vol. 52, no. 2, pp. 106–113, February 2014.

[2] Z. Pi and F. Khan, "An introduction to millimeter-wave mobile broadband systems," *IEEE Communications Magazine*, no. 6, pp. 101–107, 2011.

[3] E. Ben-Dor, T. Rappaport, Y. Qiao, and S. Lauffenburger, "Millimeter-wave 60 ghz outdoor and vehicle aoa propagation measurements using a broadband channel sounder," in *IEEE GLOBECOM*, 2011.

[4] M. Samimi, K. Wang, Y. Azar, G. Wong, R. Mayzus, H. Zhao, J. Schulz, S. Sun, F. Gutierrez, and T. Rappaport, "28 ghz angle of arrival and angle of departure analysis for outdoor cellular communications using steerable beam antennas in new york city," in *IEEE VTC-Spring*, June 2013.

[5] METIS, Mobile and wireless communications Enablers for the Twenty-twenty Information Society, *D1.2, Initial channel models based on measurements*. [Online]. Available: http://www.metis2020.com

[6] MiWEBA, Millimetre-Wave Evolution for Backhaul and Access, *D5.1, Channel Modeling and Characterization*. [Online]. Available: http://www.miweba.eu

[7] S. Hur, Y.-J. Cho, J. Lee, N.-G. Kang, J. Park, and H. Benn, "Synchronous channel sounder using horn antenna and indoor measurements on 28 ghz," in *IEEE International Black Sea Conference on Communications and Networking (BlackSeaCom)*, May 2014.

[8] Kyösti, et al., "WINNER II Channel Models, ver 1.1," IST-WINNER D1.1.2 P, Sep. 2007. [Online]. Available: https://www.ist-winner.org/WINNER2-Deliverables/D1.1.2v1.1.pdf

[9] "Further advancements for E-UTRA physical layer aspects," 3GPP TR 36.814 V9.0.0, Mar. 2010.

[10] G. R. M. Jr., M. K. Samimi, and T. S. Rappaport, "Omnidirectional path loss models in new york city at 28 ghz and 73 ghz," in *IEEE 25th International Symposium on Personal Indoor and Mobile Radio Communications (PIMRC), 2014*, Sep 2014.

[11] V. Erceg, L. Greenstein, S. Tjandra, S. Parkoff, A. Gupta, B. Kulic, A. Julius, and B. Bianchi, "An emperically based pathloss model for wireless channels in surburban environments," in *IEEE Journal on Selected Areas in Communications*, vol. 17, no. 7, July 1999, pp. 1205–1211.

[12] S. Ghassemzadeh, R. Jana, C. Rice, W. Turin, and V. Tarokh, "A statistical path loss model for in-home uwb channels," in *IEEE Conference on Ultra Wideband Systems and Technoloies*, 2002, pp. 59–64.

[13] Kyösti, et al., "WINNER II Channel Models Part II, Radio Channel Measurement and Analysis Results, ver 1.1," IST-WINNER D1.1.2 P, Sep. 2007.

[14] Y. Cho, S. Hur, J. Ko, J. Park, A. F. Molisch, K. Haneda, and M. Peter, "Wideband Spatial Channel Model in an In-Buliding, Campus and Urban Cellular Environments At 28 GHz," *in preparation*.